Effect of the combined action of Faradaic currents and mobility differences in ac electro-osmosis

A. González,[1,*] A. Ramos,[2] P. García-Sánchez,[2] and A. Castellanos[2]
[1]*Depto. Física Aplicada III, Universidad de Sevilla, Camino de los Descubrimientos s/n, 41092 Sevilla, Spain*
[2]*Depto. Electrónica y Electromagnetismo, Universidad de Sevilla, Reina Mercedes s/n, 41012 Sevilla, Spain*
(Received 22 July 2009; published 28 January 2010)

In this work, we extend previous analyses of ac electro-osmosis to account for the combined action of two experimentally relevant effects: (i) Faradaic currents from electrochemical reactions at the electrodes and (ii) differences in ion mobilities of the electrolyte. In previous works, the ac electro-osmotic motion has been analyzed theoretically under the assumption that only forces in the diffuse (Debye) layer are relevant. Here, we first show that if the ion mobilities of a 1-1 aqueous solution are different, the charged zone expands from the Debye layer to include the diffusion layer. We later include the Faradaic currents and, as an attempt to explore both factors simultaneously, we perform a thin-layer, low-frequency, linear analysis of the system. Finally, the model is applied to the case of an electrolyte actuated by a traveling-wave signal. A steady liquid motion in opposite direction to the applied signal is predicted for some ranges of the parameters. This could serve as a partial explanation for the observed flow reversal in some experiments.

DOI: 10.1103/PhysRevE.81.016320 PACS number(s): 47.61.−k, 47.57.jd, 82.45.−h, 85.85.+j

I. INTRODUCTION

Alternating electric fields can generate a net steady motion of aqueous saline solutions over microelectrode structures. The term *ac electro-osmosis* (ACEO) [1–3] refers to the fluid motion generated on top of electrodes by the interaction between an ac electric field and the electrical charge that this field induces at the electrode/electrolyte interface—i.e., the charge induced in the electrical double layer (DL). ACEO flows are receiving growing interest in microfluidic applications because the integration of microelectrodes into microchannels makes possible the local actuation of electrolytes by means of electric fields [4,5]. Unidirectional fluid flow using ACEO has been demonstrated using either arrays of asymmetric electrodes energized by a single ac signal [6,7] or arrays of symmetric electrodes energized by a traveling-wave (TW) signal [8,9]. Bazant and Squires [10,11] analyzed different fluid flows originated by electric fields acting upon the induced charge in the double layer of polarizable objects and suggested the term *induced-charge electro-osmosis* to include all these phenomena.

The mechanism responsible for fluid pumping in the case of microelectrodes actuated by a traveling-wave signal of small amplitude is shown in Fig. 1. In experiments, the TW potential is typically generated using a four-phase ac signal applied to successive quadruplets of electrodes (Fig. 1, left). After application of a TW potential to the electrodes, counterions accumulate in the double layer at the interfaces between electrodes and electrolyte. The induced charge in the double layer lags behind the applied signal due to the finite charging time of the double layer. The ions are, therefore, subjected to a tangential electrical force in the direction of the traveling wave that, by viscous friction, is transmitted to the fluid. The characteristic charging time of the double layer is given by the product of the typical resistance of the bulk $L/\sigma S$ and the typical capacitance of the double layer $\varepsilon S/\lambda_D$, $t_c=(\varepsilon/\sigma)(L/\lambda_D)$. Here, ε and σ are the permittivity and conductivity of the liquid, respectively, L and S denote the typical length and area of the system, and λ_D is the Debye length. This charging time typically lies in the range of milliseconds. If the period of the applied signal, T, is very large compared to t_c counterions have time to accumulate in the double layer. The electrical force is, then, mainly normal to the surface and negligible flow occurs. If the period of the applied signal T is much shorter than t_c the accumulation of induced charge in the double layer becomes negligible and, again, no lateral motion is generated. Maximum lateral force and fluid flow occur for $T\sim t_c$, which typically corresponds to an applied frequency in the range of kilohertz.

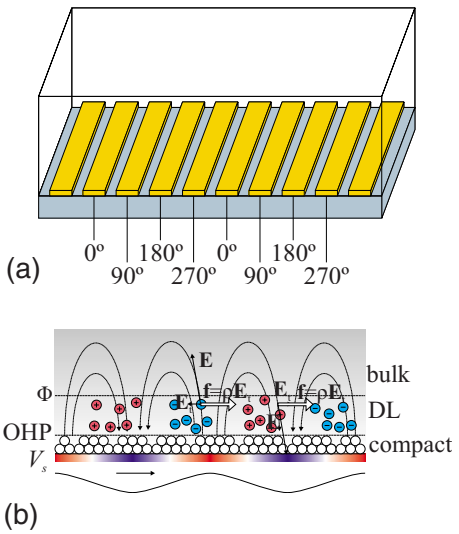

FIG. 1. (Color online) (a) Diagram showing a microelectrode array subjected to a four-phase ac signal to produce a traveling-wave potential. (b) Scheme of traveling-wave electro-osmosis (TWEO) mechanism: the induced charge in the DL lags behind the applied signal due to the finite DL charging time. The tangential field produces a force in the direction of the wave for both positive and negative ions, resulting in steady liquid motion.

*Corresponding author; gonfer@us.es

The simplest form of ac electro-osmosis theory [1,2] is a linear theory (valid for small applied voltage) that assumes that only forces in the diffuse layer are present and that the electrodes are perfectly polarizable, i.e., there are no Faradaic currents. In most cases, the predictions of the ACEO theory reasonably explain experimental observations at voltages smaller than 5 $V_{p.p.}$ when using pairs of symmetric electrodes [3,12], as well as those observations at voltages smaller than 2–3 $V_{p.p.}$ with arrays of electrodes [6–9,13]. However, the theory also presents many quantitative discrepancies with observations and, for certain ranges of liquid conductivity, frequency, and voltage, even the direction of the liquid motion is opposite to the ACEO prediction (*flow reversal*) [7,9,13,14].

Recently, the effects of the finite size of ions (crowding effects) have been included into the Poisson-Boltzmann equation [15,16]. This model has yielded a possible explanation [17] for the flow reversal observed by Studer *et al.* with arrays of electrodes of different widths [7]. For this prediction, it is essential that electrodes of different widths show different charging times due to nonlinear crowding effects. This reasoning is not valid for arrays of electrodes subjected to traveling-wave potentials, where all electrodes have the same width.

Another aspect of the experiments at larger applied potentials is that the assumption of perfectly polarizable electrodes is not valid anymore and Faradaic currents occur. Olesen *et al.* [18] and Ramos *et al.* [19] generalized the ACEO theory by considering Faradaic reactions at the electrodes. These works only considered forces inside the Debye layer and, as a general result, obtained that Faradaic currents depolarize the electrode-electrolyte interface leading to lower electro-osmotic velocities. In a recent work, García-Sánchez *et al.* [20] showed that Faradaic currents occur in TWEO experiments for applied signals typical of flow reversal. In some cases, the electrical current variation in time was clearly correlated with the observed flow reversal in these TWEO arrays. García-Sánchez *et al.* showed in further experiments [21] that electrochemical reactions lead to a decrement of *p*H near electrodes. The concentration of H^+ increases and it can become comparable or even larger than the concentrations of ions coming from the salt (KCl at a concentration of 0.1 mM). The mobility of H^+ is much higher than that of K^+ or Cl^- and, therefore, the implicit assumption made in previous ACEO models that the difference in mobility of ionic species was unimportant may result too simplistic. García-Sánchez *et al.* [21] also reported oscillations of total ionic concentration close to the electrodes originated by Faradaic currents for voltage amplitudes of 6 $V_{p.p.}$ at low frequencies. The penetration length of these oscillations behaved as $l(\omega) \approx (D/\omega)^{1/2}$ (where D is a diffusion constant), which is expected for a diffusion layer. In addition, they presented preliminary numerical computations of electrically induced fluid flows for the case of two ionic species with different mobilities. These computations took into account specifically the induced charge and electrical force outside the Debye layer in the diffusion layer. They showed that the electric field acting on the charge induced in the diffusion layer can lead to reverse flow, although the motion generated in the Debye layer was completely ignored in these computations.

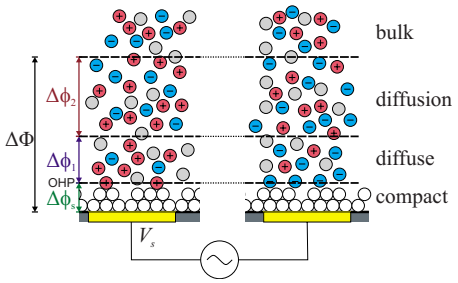

FIG. 2. (Color online) Structure of the extended double layer (XDL) on an array of electrodes subjected to an ac potential. Three distinct layers are indicated: compact layer (formed by fixed adsorbed ions and water molecules), diffuse layer (where thermal and electric forces are of the same order), and diffusion layer (associated to the finite diffusion penetration length for the different species). The outer Helmholtz plane (OHP) is localized between the compact and diffuse layers.

Motivated by this, we aim to extend previous theoretical analysis of Faradaic currents in ACEO by considering a 1-1 electrolyte with ions of different mobilities. The paper is organized as follows. First, we present the mathematical model and approximations to the problem. We then obtain a generalized boundary condition for the electrical potential on electrodes. Subsequently, we derive a general expression for the electro-osmotic slip velocity that accounts for the stresses in the Debye and diffusion layers. Finally, we apply the model to the particular case of a single mode traveling-wave potential. The model predicts flow reversal for the specific conditions of a compact layer thickness of the order of the Debye length or greater, facile Faradaic currents, and a large asymmetry in ion mobilities.

II. MATHEMATICAL MODEL

We consider a 1:1 aqueous solution X^+Y^- (e.g., Na^+Cl^- or K^+Cl^-) placed on top of an array of electrodes subjected to an ac signal (Fig. 2). We are mostly interested in the behavior of the system close to the plane of the electrodes. Above this plane, following previous models [22] we distinguish three distinct layers: compact, diffuse, and diffusion. ac electro-osmosis is usually explained in terms of the phenomena that happen in the combination of compact and diffuse layers (known as electric double layer, abbreviated as EDL). In this paper, we also examine the effect of the charges situated in the diffusion layer. Because of this, we use the expression "extended double layer," hereafter referred as XDL, to the combination of the three layers.

In our model we only include two charged species and consider the pair of ions to be *asymmetric* in the sense that their mobilities are different. For simplicity, we assume that the cations react reversibly at the electrodes to produce neutral molecules according to a simple one-step one-electron redox process of the form $X^+ + e^- \leftrightarrow X$ and that the electrodes are blocking for the anions. The sign of the reacting species, however, is not essential to the model. The introduction of the chemical reaction requires the inclusion of one neutral species, X, in the mathematical analysis.

In our system, there is an ac applied voltage on the electrodes and this signal induces charges and motion in the liquid. Hence, we are interested not in the total voltage drop across the XDL but only in the excess over the equilibrium dc voltage. For simplicity, we will assume that dc equilibrium voltage is very small and can be neglected. The behavior of our system can be modeled in terms of four functions: the electric potential, ϕ, and the densities of positive, negative, and neutral species, c_+, c_-, and c_0, respectively. Our model describes a two-dimensional system, which approximates the behavior of a solution on top of an array of electrodes in the form of long strips. We denote as x the coordinate tangential to the plane of the electrodes and as y the coordinate normal to this plane. The different quantities verify the Poisson-Nernst-Planck (PNP) equations in the half-plane $y>0$, with boundary conditions at the OHP, $y=0$ [23].

The electric potential obeys Poisson's equation,

$$\nabla^2\phi = -\frac{e}{\varepsilon}(c_+ - c_-), \tag{1}$$

while the particle densities satisfy Nernst-Planck equations,

$$\frac{\partial c_+}{\partial t} + \nabla\cdot\mathbf{F}_+ = 0, \quad \mathbf{F}_+ = \mu_+ c_+\mathbf{E} - D_+\nabla c_+ + c_+\mathbf{v}, \tag{2}$$

$$\frac{\partial c_-}{\partial t} + \nabla\cdot\mathbf{F}_- = 0, \quad \mathbf{F}_- = -\mu_- c_-\mathbf{E} - D_-\nabla c_- + c_-\mathbf{v}, \tag{3}$$

$$\frac{\partial c_0}{\partial t} + \nabla\cdot\mathbf{F}_0 = 0, \quad \mathbf{F}_0 = -D_0\nabla c_0 + c_0\mathbf{v}. \tag{4}$$

The diffusion coefficients and ionic mobilities are related through the Einstein relation: $D_+/\mu_+ = D_-/\mu_- = k_B T/e$, where k_B is the Boltzmann constant, T is the absolute temperature, and e is the elementary charge.

To these equations we must add the Stokes equation for the liquid motion,

$$\nabla\cdot\mathbf{v} = 0, \tag{5}$$

$$\mathbf{0} = -\nabla p + \eta\nabla^2\mathbf{v} + \rho\mathbf{E}, \tag{6}$$

with $\rho = e(c_+ - c_-)$.

The boundary conditions at the OHP ($y=0$) for these functions are the continuity of the displacement vector, assuming a linear compact layer of width λ_s and permittivity ε_s [19,24],

$$\frac{\varepsilon_s}{\lambda_s}\Delta\phi_s = -\varepsilon\frac{\partial\phi}{\partial y}, \tag{7}$$

where $\Delta\phi_s$ denotes the voltage drop across the compact layer (Fig. 2),

$$\Delta\phi_s = V_s(x,t) - \phi(y=0). \tag{8}$$

We assume that the electrodes are blocking to the anions,

$$0 = \mathbf{u}_y\cdot\mathbf{F}_- = \mu_- c_-\frac{\partial\phi}{\partial y} - D_-\frac{\partial c_-}{\partial y}, \tag{9}$$

whereas the fluxes of positive and neutral species are related through Faradaic currents,

$$-\mu_+ c_+\frac{\partial\phi}{\partial y} - D_+\frac{\partial c_+}{\partial y} = \frac{J_F}{e}, \tag{10}$$

$$-D_0\frac{\partial c_0}{\partial y} = -\frac{J_F}{e}. \tag{11}$$

To model this current we use the Butler-Volmer equation [23–25],

$$\frac{J_F}{e} = K_0 c_0\exp\left(\frac{\beta e\Delta\phi_s}{k_B T}\right) - K_+ c_+\exp\left(-\frac{(1-\beta)e\Delta\phi_s}{k_B T}\right), \tag{12}$$

with β as the *transfer coefficient*, where the reaction constants K_0 and K_+ are related by the equilibrium condition $K_0 c_0^{eq} = K_+ c_+^{eq}$. In this equation, we introduce the Frumkin correction [25] from the beginning and assume that the voltage drop that appears in Eq. (12) corresponds to the one between the electrodes and the OHP (Fig. 2) [24]. Note that we do not consider effects due to the adsorption of movable ions.

The boundary condition for the liquid velocity at the OHP is the no-slip condition

$$\mathbf{v} = \mathbf{0}. \tag{13}$$

The equations can be made dimensionless using adequate scales. We choose the following: the equilibrium concentrations c^{eq} for the charged species and c_0^{eq} for the neutral species; the thermal voltage $k_B T/e$ for the electric potential; the Debye length λ_D for the normal (y) coordinate, with the Debye length given by $(\varepsilon k_B T/2e^2 c^{eq})^{1/2}$; a typical macroscopic length L for the tangential (x) coordinate (for instance, in the case of a traveling-wave signal, L is of the order of the wavelength); the reciprocal of the angular frequency, $1/\omega$, for the time; $2ec^{eq}D_+/\lambda_D$ for the current density; $\varepsilon(k_B T/e)^2/\eta L$ for the liquid velocity; and $\varepsilon(k_B T/e\lambda_D)^2$ for the pressure.

Instead of the ionic concentrations, we will use as unknowns the charge density ρ and the mean ion concentration $c=(c_+ + c_-)/2$, defined in dimensionless form as $\bar{\rho} = (\bar{c}_+ - \bar{c}_-)/2$ and $\bar{c} = (\bar{c}_+ + \bar{c}_-)/2$.

Using these scales the complete system is written in dimensionless form as

$$\delta^2\frac{\partial^2\bar{\phi}}{\partial\bar{x}^2} + \frac{\partial^2\bar{\phi}}{\partial\bar{y}^2} = -\bar{\rho}, \tag{14}$$

$$\left[\bar{\omega}\frac{\partial}{\partial\bar{t}} + \mathrm{Pe}\left(\bar{u}\frac{\partial}{\partial\bar{x}} + \bar{w}\frac{\partial}{\partial\bar{y}}\right)\right](\bar{\rho} - \gamma\bar{c}) = \frac{\partial}{\partial\bar{y}}\left(\bar{c}\frac{\partial\bar{\phi}}{\partial\bar{y}} + \frac{\partial\bar{\rho}}{\partial\bar{y}}\right) + \delta^2\frac{\partial}{\partial\bar{x}}\left(\bar{c}\frac{\partial\bar{\phi}}{\partial\bar{x}} + \frac{\partial\bar{\rho}}{\partial\bar{x}}\right), \tag{15}$$

TABLE I. Values of the parameter $\gamma=(D_+-D_-)/(D_++D_-)$ for some ion pairs.

γ	K^+	Na^+	H^+
Cl^-	−0.019	−0.207	+0.642
OH^-	−0.459	−0.596	+0.277

$$\left[\bar{\omega}\frac{\partial}{\partial \bar{t}}+\mathrm{Pe}\left(\bar{u}\frac{\partial}{\partial \bar{x}}+\bar{w}\frac{\partial}{\partial \bar{y}}\right)\right](\bar{c}-\gamma\bar{\rho})$$
$$=\frac{\partial}{\partial \bar{y}}\left(\bar{\rho}\frac{\partial \bar{\phi}}{\partial \bar{y}}+\frac{\partial \bar{c}}{\partial \bar{y}}\right)+\delta^2\frac{\partial}{\partial \bar{x}}\left(\bar{\rho}\frac{\partial \bar{\phi}}{\partial \bar{x}}+\frac{\partial \bar{c}}{\partial \bar{x}}\right), \quad (16)$$

$$\left[\bar{\omega}\frac{\partial}{\partial \bar{t}}+\mathrm{Pe}\left(\bar{u}\frac{\partial}{\partial \bar{x}}+\bar{w}\frac{\partial}{\partial \bar{y}}\right)\right]\bar{c}_0=\bar{D}_0\left(\frac{\partial^2 \bar{c}_0}{\partial \bar{y}^2}+\delta^2\frac{\partial^2 \bar{c}_0}{\partial \bar{x}^2}\right), \quad (17)$$

$$\frac{\partial \bar{u}}{\partial \bar{x}}+\frac{\partial \bar{w}}{\partial \bar{y}}=0, \quad (18)$$

$$0=-\frac{\partial \bar{p}}{\partial \bar{x}}+\delta^2\frac{\partial^2 \bar{u}}{\partial \bar{x}^2}+\frac{\partial^2 \bar{u}}{\partial \bar{y}^2}-\bar{\rho}\frac{\partial \bar{\phi}}{\partial \bar{x}}, \quad (19)$$

$$0=-\frac{\partial \bar{p}}{\partial \bar{y}}+\delta^2\frac{\partial^2 \bar{w}}{\partial \bar{y}^2}+\delta^4\frac{\partial^2 \bar{w}}{\partial \bar{x}^2}-\bar{\rho}\frac{\partial \bar{\phi}}{\partial \bar{y}}. \quad (20)$$

The boundary conditions at $\bar{y}=0$ are

$$\Delta\bar{\phi}_s=-\bar{\lambda}_s\frac{\partial \bar{\phi}}{\partial \bar{y}}, \quad \Delta\bar{\phi}_s=\bar{V}_s(\bar{x},\bar{t})-\bar{\phi}(\bar{y}=0), \quad (21)$$

$$-\bar{c}\frac{\partial \bar{\phi}}{\partial \bar{y}}-\frac{\partial \bar{\rho}}{\partial \bar{y}}=\bar{J}_F, \quad -\bar{\rho}\frac{\partial \bar{\phi}}{\partial \bar{y}}-\frac{\partial \bar{c}}{\partial \bar{y}}=\bar{J}_F,$$
$$-\bar{D}_0(1-\gamma)\frac{\partial \bar{c}_0}{\partial \bar{y}}=-N\bar{J}_F, \quad (22)$$

$$\bar{J}_F=G\{\bar{c}_0\exp(\beta\Delta\bar{\phi}_s)-(\bar{c}+\bar{\rho})\exp[-(1-\beta)\Delta\bar{\phi}_s]\}, \quad (23)$$

$$\bar{u}=0, \quad \bar{w}=0. \quad (24)$$

This system depends on a set of dimensionless parameters[1]:

(i) Asymmetry: $\gamma=(D_+-D_-)/(D_++D_-)=(\mu_+-\mu_-)/(\mu_++\mu_-)$. The parameter γ measures the asymmetry of the solution, ranging from −1 (immobile cations) to +1 (immobile anions); for $\gamma=0$ we have a complete symmetric electrolyte. The values for some common ion pairs are provided in Table I (using data from [28]).

(ii) Diffuse layer thickness: $\delta=\lambda_D/L$. This parameter measures the thickness of the diffuse layer (the Debye length) compared to the typical macroscopic length. For an experiment using electrodes in the range of tens of microns, this parameter is usually very small, in the range of 10^{-3} (since the Debye length can be in the range of tens of nanometers while the electrodes have tens of microns). In what follows we will take $\delta=0.001$ in the numerical calculations except otherwise indicated.

(iii) Compact layer thickness: $\bar{\lambda}_s=(\varepsilon/\lambda_D)/(\varepsilon_s/\lambda_s)$ gives the ratio between the capacitance of the diffuse layer to the compact layer. This can be interpreted as a ratio between effective thicknesses: $\bar{\lambda}_s=(\varepsilon\lambda_s/\varepsilon_s)/\lambda_D$.

(iv) Frequency: $\bar{\omega}=\omega\lambda_D^2/D$ scales the frequency of the applied signal in terms of the relaxation frequency of the solution. Here D is the ambipolar diffusivity, defined as $D=2D_+D_-/(D_++D_-)$ [22]. The dimensionless frequency is usually small in the case of ac electro-osmotic flow, of order δ or smaller in most experimental cases. Because of this, it is useful to introduce a rescaled frequency, $\Omega=(\omega\varepsilon/\sigma)(L/\lambda_D)=\bar{\omega}(1-\gamma^2)/\delta$, which is typically of order unity in the ACEO regime. This frequency Ω uses the relaxation time of the *RC* circuit formed by the double layer capacitance and the bulk resistance.

(v) Voltage amplitude: $\bar{V}_0=eV_0/k_BT$ measures the applied voltage. Since k_BT/e is approximately 25 mV, typical values of the dimensionless amplitude can be in the range of 10^1-10^2.

(vi) Reaction conductance: $G=\lambda_DK_+/2D_+=\lambda_D/R_{ct}\sigma(1+\gamma)$, with R_{ct} as the specific charge transfer resistance for the Faradaic reactions $R_{ct}=k_BT/c^{eq}e^2K_+$. It measures the facility of the chemical reaction. The changes in this parameter become important when the charge transfer is comparable to the bulk specific resistance ($R_{ct}\sim L/\sigma$). Because of this, a more meaningful combination is the ratio $G/\delta=L/R_{ct}\sigma(1+\gamma)$ (typical bulk resistance divided by charge transfer resistance). A small value of G/δ means that the reaction at the electrodes is blocked, while a large value gives the *facile kinetic regime*, for which the chemical reaction is almost at equilibrium. We also use the dimensionless reaction resistance defined as $R_s=1/G$, proportional to R_{ct}.

(vii) Neutral species diffusivity: $\bar{D}_0=D_0/D$ measures the diffusivity of the neutral species compared to the ambipolar diffusivity.

(viii) Relative concentration: $N=2c^{eq}/c_0^{eq}$ measures the fraction of charged species compared to the neutral one. A small value of N corresponds to a bath of neutral species. A large value of N implies that there are little neutral species available.

(ix) Péclet number: $\mathrm{Pe}=u_0\lambda_D^2/LD$ gives the importance of the advective currents to the diffusion currents inside the double layer.

In what follows, unless otherwise noted, we will assume that all quantities are nondimensional and drop the overbars.

III. APPROXIMATIONS

We are interested mainly in the solution for the electromechanical problem inside the diffuse and diffusion layers in

[1]The transfer coefficient β will disappear in our linear analysis and we do not include it on the list of dimensionless parameters.

order to obtain integrated boundary conditions for the problem in the bulk. To achieve this, we make a series of assumptions:

Negligible advective currents. The role of advection might be important in the bulk, but inside the double layer typical values of the Péclet number are in the range of 10^{-6}. Inside the diffusion layer the typical length is proportional to $\omega^{-1/2}$ and the effective Péclet number inside this layer, for typical values of the frequency in ac electro-osmosis, is $\mathrm{Pe}'=\mathrm{Pe}/\omega \sim 10^{-3}$, which is still very small. In addition, we will assume that the diffusion coefficient for the neutral species is not so low that advection becomes the dominant factor in the species dispersion. This allows us to neglect advection and omit the corresponding terms in Eqs. (15)–(17) as long as y is moderate. With this approximation the electrical problem decouples from the mechanical one, and we can solve first for the electric potential, charge density, and mean concentration and use the resulting force to calculate the liquid velocity.

Linearization of PNP equations. The system can be linearized expanding the quantities in powers of V_0. This choice may be questionable since the parameter V_0 can be in the range of 40 or more. Because of this, we must understand the following results as a partial explanation of the mechanisms underlying ac electro-osmosis with Faradaic currents. A complete analysis must be fully nonlinear.

For the concentrations we have the perturbations over the equilibrium state, while the electric potential and the charge density vanish at zero order,

$$\phi = O(V_0), \quad \rho = O(V_0), \tag{25}$$

$$c = 1 + n, \quad n = O(V_0), \quad c_0 = 1 + n_0, \quad n_0 = O(V_0). \tag{26}$$

The linearization of the system allows us to use complex amplitudes (phasors) as the applied signal is of the form

$$V_s(x,t) = V_s(x)e^{it} + V_s^*(x)e^{-it} = 2\ \mathrm{Re}[V_s(x)e^{it}]. \tag{27}$$

In the particular case of a single mode traveling wave $V_s(x,t)=V_0\cos(t-x)$ and $V_s(x)=V_0\exp(-ix)/2$. As responses to this signal, ϕ, ρ, n, and n_0 admit a similar expansion to Eq. (27).

Since the equilibrium dc voltage is assumed to be zero, the liquid velocity is generated by the coupling of the time-varying charge with the ac electric potential and thus is quadratic in V_0, $\mathbf{v}=O(V_0^2)$. The same happens with the pressure, $p=O(V_0^2)$. The resulting liquid velocity and pressure will be a combination of terms oscillating with twice the frequency of the applied signal plus a time-independent term. We will be interested in the latter term because it means steady liquid motion, the one usually observed in experiments.

Thin layer approximation. The following approximation consists in taking into account that both the Debye length, λ_D, and the diffusion layer thickness (proportional to $\omega^{-1/2}$) are much smaller than the typical transversal length, L. In terms of the parameters, this means that $\delta \ll 1$ and ω is not much smaller than δ^2.

With this approximation we can neglect terms of order δ^2 in the system as, for example, the second derivatives in the tangential coordinate, x. As a consequence, the dependences on x and y decouple and the electrical problem inside the XDL becomes effectively one-dimension, acting the tangential coordinate as a parameter.

To complete the one-dimensional problem we need boundary conditions for y going to infinity, which physically means moving outside the XDL to the bulk. We assume that in this limit the concentrations tend to their equilibrium values and the liquid becomes electroneutral,

$$n \to 0, \quad \rho \to 0, \quad n_0 \to 0, \tag{28}$$

while the electric potential matches asymptotically its value in the bulk. To perform the asymptotic matching we define an outer normal coordinate $y_o=\delta y$, scaled using the same macroscopic length L that we used to scale x. If Φ is the outer electric potential, the matching implies (see Appendix A for a geometrical explanation)

$$\lim_{\substack{y\to\infty \\ y_o\to 0}} \left(\frac{1}{\delta}\frac{\partial \phi}{\partial y} - \frac{\partial \Phi}{\partial y_o} \right) = 0, \tag{29}$$

$$\lim_{\substack{y\to\infty \\ y_o\to 0}} \left[\left(\phi - y\frac{\partial \phi}{\partial y} \right) - \left(\Phi - y_o\frac{\partial \Phi}{\partial y_o} \right) \right] = 0. \tag{30}$$

These matching relations will allow us to obtain a Robin-type boundary condition, $\alpha\Phi+\beta\mathbf{n}\cdot\nabla\Phi=f$, for the outer potential once we have solved the inner problem.

Taking into account all the approximations we obtain the following set of linear equations for the electrical problem inside the XDL:

$$\frac{\partial^2 \phi}{\partial y^2} = -\rho, \tag{31}$$

$$\frac{\partial^2 \rho}{\partial y^2} = (1 + i\omega)\rho - i\omega\gamma n, \tag{32}$$

$$\frac{\partial^2 n}{\partial y^2} = -i\omega\gamma\rho + i\omega n, \tag{33}$$

$$\frac{\partial^2 n_0}{\partial y^2} = \frac{i\omega}{D_0} n_0. \tag{34}$$

One particular combination of Eqs. (31)–(33) that is especially useful to determine the solution is the charge conservation equation,

$$\frac{\partial^2}{\partial y^2}\{[1 + i\omega(1-\gamma^2)]\phi + \rho + \gamma n\} = 0. \tag{35}$$

The linear boundary conditions at $y=0$ for the complex amplitudes are

$$\Delta\phi_s = -\lambda_s \frac{\partial \phi}{\partial y}, \quad \Delta\phi_s = V_s(x) - \phi(y=0), \tag{36}$$

$$-\frac{\partial \phi}{\partial y}-\frac{\partial \rho}{\partial y}+\frac{\partial n}{\partial y}=0, \quad -\frac{\partial n}{\partial y}=J_F,$$

$$-D_0(1-\gamma)\frac{\partial n_0}{\partial y}-N\frac{\partial n}{\partial y}=0, \tag{37}$$

$$J_F=G(n_0-n-\rho+\Delta\phi_s). \tag{38}$$

Low frequency range. Experiments show that the maximum velocity is obtained at low frequencies, of order δ [in our case, a typical value of δ is 0.001, which corresponds to a dimensional frequency: $(\sigma/\varepsilon)(\lambda_D/L)\sim 10^3$ rad/s or smaller]. Because of this, in our analysis we will be interested in dimensionless frequencies much smaller than unity, so that the system behaves quasistatically. In addition to the complete linear solution, we will perform an expansion in powers of ω in order to provide results which are more easily interpreted. The low-frequency domain of these asymptotic solutions has a lower bound since ω must not be so low that the diffusion layer thickness becomes of the order of the macroscopic length. In terms of the parameters, this means that ω must not be much smaller than δ^2.

Looking at Eqs. (31)–(34), we can see that for $\omega \ll 1$ the different concentrations decay mainly along different distances: the charge density decays along a length unity (i.e., the Debye length in the double layer), the excess on the mean concentration along a length proportional to $\omega^{-1/2}$ (the diffusion layer), and similarly for the neutral species $(\omega/D_0)^{-1/2}$.

IV. SOLUTION INSIDE THE XDL

A. Complete linear system in the thin-layer approximation

Equations (31)–(34) can be solved for the four functions, resulting in a combination of exponentials,

$$\phi=(f_1e^{-s_1y}+f_2e^{-s_2y}-Y)\Delta\Phi(x)+\Phi_0(x), \tag{39}$$

$$\rho=(\rho_1e^{-s_1y}+\rho_2e^{-s_2y})\Delta\Phi(x), \tag{40}$$

$$n=(n_1e^{-s_1y}+n_2e^{-s_2y})\Delta\Phi(x), \tag{41}$$

$$n_0=a_0e^{-s_0y}\Delta\Phi(x). \tag{42}$$

In these equations, we have factored out the dependence on the tangential coordinate and introduced the total voltage drop across the XDL so that the individual voltage drop across the compact, diffuse, and diffusion layers can be expressed as fractions of the total voltage drop (Fig. 2),

$$\Delta\phi_s=f_s\Delta\Phi, \quad \Delta\phi_{\text{diffuse}}=f_1\Delta\Phi, \quad \Delta\phi_{\text{diffusion}}=f_2\Delta\Phi, \tag{43}$$

$$f_s+f_1+f_2=1, \tag{44}$$

where f_1, f_2, and f_s are *complex* quantities. The Faradaic current density J_F can also be expressed as

$$J_F=j_F\Delta\Phi. \tag{45}$$

The decay factors for the three exponentials are

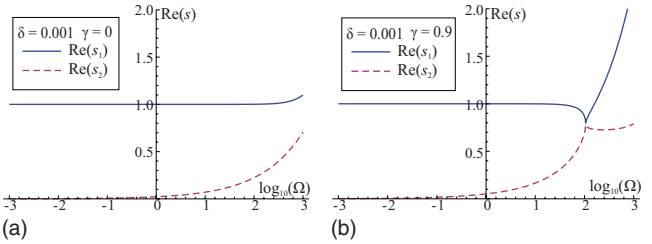

FIG. 3. (Color online) Real part of the decay factors for (a) an aqueous solution with equal ion mobilities and (b) one with very different ones. The eigenvalues have been plotted against the rescaled frequency $\Omega=\omega(1-\gamma^2)/\delta$. For equal ion mobilities, the decay lengths (thicknesses of the diffuse and diffusion layers) are distinct, but for highly asymmetrical diffusion they are closer and can even intersect: the distinction between the layers vanishes.

$$s_1=\sqrt{\Gamma+i\omega}=1+O(\omega),\ \mathrm{Re}(s_1)>0 \quad \text{with}$$

$$\Gamma=(1+\sqrt{1-4\gamma^2\omega^2})/2, \tag{46}$$

$$s_2=\sqrt{1+i\omega-\Gamma}=\sqrt{i\omega}+O(\omega^{3/2}),\ \mathrm{Re}(s_2)>0, \tag{47}$$

$$s_0=\sqrt{\frac{i\omega}{D_0}},\ \mathrm{Re}(s_0)>0. \tag{48}$$

For low frequencies the exponent s_1 tends to unity (i.e., the dimensional decay length is the Debye length) while s_2 goes as $(i\omega)^{1/2}$, which is proportional to the reciprocal of the diffusion length for the charged species. The last exponent gives the diffusion length for the neutral species. According to these behaviors, we can associate f_1 with the voltage drop across the diffuse layer and f_2 with the one across the diffusion layer. Nevertheless, for high values of the asymmetry γ and frequency, the two factors actually cross (Fig. 3) and the two layers cease to be distinct. For γ=0.64 (case of H^+Cl^-) and δ=0.001, this occurs at the (dimensional) frequency $\omega=0.46\sigma/\varepsilon$.

In Eq. (39) the electric potential includes a term independent of y, $\Phi_0(x)$, and a linear one, $[-Y\Delta\Phi(x)]y$. These two terms work as boundary conditions for the outer electric potential. Using the matching conditions (29) and (30) we obtain for the outer potential

$$\lim_{y_o\to 0}\left(\frac{\partial\Phi}{\partial y_o}\right)=\lim_{y\to\infty}\left(\frac{1}{\delta}\frac{\partial\phi}{\partial y}\right)=-\frac{Y}{\delta}\Delta\Phi, \tag{49}$$

$$\lim_{y_o\to o}(\Phi)=\lim_{y\to\infty}\left(\phi-y\frac{\partial\phi}{\partial y}\right)=\Phi_0. \tag{50}$$

Using that $\Delta\Phi=V_s-\Phi_0$, we can reduce the two matching conditions to a single Robin boundary condition for the outer potential,

$$-\delta\frac{\partial\Phi}{\partial y_o}=Y\Delta\Phi, \quad \Delta\Phi=V_s-\Phi \quad (y_o=0). \tag{51}$$

The quantity Y represents the ratio between the current density that goes through the XDL and the voltage drop across

this layer. This quantity can be understood as the (dimensionless) specific admittance of the XDL.

Substituting in the differential equations we obtain the algebraic equations that relate the coefficients

$$[1+i\omega(1-\gamma^2)]f_1+\rho_1+\gamma n_1=0, \tag{52}$$

$$[1+i\omega(1-\gamma^2)]f_2+\rho_2+\gamma n_2=0, \tag{53}$$

$$\Gamma n_1+i\omega\gamma\rho_1=0, \tag{54}$$

$$\Gamma\rho_2-i\omega\gamma n_2=0, \tag{55}$$

where Γ is defined in Eq. (46).

From Eq. (55), if the system is symmetrical ($\gamma=0$) the charge exists only in the diffuse layer since $\rho_2=0$. Moreover, for a completely symmetrical electrolyte the excess in the mean concentration decays only in the diffusion layer as $n_1=0$ from Eq. (54). The presence of asymmetry implies that there is a charge density inside the diffusion layer, which must be taken into account to calculate the electro-osmotic slip velocity. For small frequencies, this charge density is small (at least of order ω) and the total charge inside the diffusion layer is also small (of order $\omega^{1/2}$), but the voltage drop f_2 associated with it (which appears in the Smoluchowski formula) may be of order unity and have a significant contribution to the slip velocity.

Substituting the solutions in the boundary conditions we get another set of algebraic equations for the coefficients

$$f_s=\lambda_s(s_1f_1+s_2f_2+Y), \tag{56}$$

$$s_1(\rho_1+f_1-n_1)+s_2(\rho_2+f_2-n_2)+Y=0, \tag{57}$$

$$s_1n_1+s_2n_2=j_F, \tag{58}$$

$$N(s_1n_1+s_2n_2)+D_0(1-\gamma)s_0a_0=0, \tag{59}$$

$$j_F=G(a_0-n_1-n_2-\rho_1-\rho_2+f_s). \tag{60}$$

In addition we have the condition on the amplitudes,

$$f_s+f_1+f_2=1. \tag{61}$$

The system of ten equations [Eqs. (52)–(61)] can be solved completely for any values of the parameters for the ten unknowns: f_1, f_2, f_s, ρ_1, ρ_2, n_1, n_2, a_0, Y, and j_F. The complete solution is included in Appendix B.

Equations (48) and (59) imply that the relative concentration N and diffusivity D_0 appear together through the combination $W_0=N/[(1-\gamma)D_0^{1/2}]$ (since there is a factor $D_0^{-1/2}$ inside the decay factor s_0). That means that reducing the concentration of the neutral species (raising N) is equivalent to lowering its diffusivity.

B. Low frequency domain

We can expand the equations and their solutions in powers of the square root of the dimensionless frequency $\omega^{1/2}$ because as already mentioned the peak in the ac electro-osmotic velocity is obtained when $\omega\sim\delta\sim0.001$ or smaller. The use of half integers instead of whole integers in the Taylor expansion is required by the presence of diffusion.

Manipulating the equations we can obtain a general expression for the admittance,

$$Y=(1+\gamma)\left(\frac{i\omega s_1(\Gamma+i\gamma\omega)}{\Gamma}f_1-\frac{s_2(\Gamma-i\gamma\omega)}{\gamma}f_2\right). \tag{62}$$

Using the low-frequency behavior for exponents (46)–(48), it results in an admittance that goes as $(i\omega)^{1/2}$ (as in a Warburg impedance) except when $f_2=0$; for this case the admittance grows as $(i\omega)$ (a capacitive behavior).

To obtain a solution valid for low and high reaction resistances, we assume temporarily, for the sake of the perturbative expansion of the complete solution, that G and $\omega^{1/2}$ are of the same order. This can be motivated physically by the known result that the changes in behavior happen when the reaction resistance is comparable to the Warburg impedance [19]. With this hypothesis, a complete analysis shows that the Faradaic current density j_F is of the same order as G. Retaining only the leading terms for each quantity the volume equations and boundary conditions reduce to

$$n_1=0,\quad \rho_2=0,\quad f_1+\rho_1=0,\quad f_2+\gamma n_2=0, \tag{63}$$

$$f_s=\lambda_s f_1,\quad Y=-\sqrt{i\omega}(1+\gamma)f_2/\gamma,\quad \sqrt{D_0}(1-\gamma)a_0+Nn_2=0,$$

$$j_F=n_2\sqrt{i\omega},\quad j_F=G(a_0-n_2-\rho_1+f_s). \tag{64}$$

Solving this system, we obtain the leading terms for the different functions,

$$f_1=\frac{1}{1+\lambda_s}\left(1+\frac{\gamma Y}{(1+\gamma)\sqrt{i\omega}}\right),\quad f_2=-\frac{\gamma Y}{(1+\gamma)\sqrt{i\omega}}, \tag{65}$$

$$Y=\frac{1}{Z},\quad Z=\frac{1}{(1+\gamma)}\left(\frac{1}{G}+\frac{W}{\sqrt{i\omega}}\right),\quad W\equiv\frac{N}{(1-\gamma)\sqrt{D_0}}+1-\gamma. \tag{66}$$

The XDL impedance Z can be written in dimensional form as

$$Z(\mathrm{dim})=\frac{\lambda_D}{\sigma}\bar{Z}=R_{ct}+\frac{k_BT}{e^2}\left(\frac{1}{c_0^{eq}\sqrt{D_0}}+\frac{(1-\gamma)^{3/2}}{2c^{eq}\sqrt{D_+}}\right)\frac{1}{\sqrt{i\omega}} \tag{67}$$

and can be read as the association in series of the specific charge transfer resistance with two Warburg impedances, one corresponding to the neutral species and one to the charged species. A similar result was also obtained by Olesen [26].

The lowest order for XDL impedance [Eq. (67)] goes to infinity when the Faradaic reactions are blocked. This can happen if $R_{ct}\to\infty$ (limit of small exchange current), c_0^{eq} or $c^{eq}\to0$ (scarce reacting species), and D_0 or $D_+\to0$ (vanishing diffusivities). In terms of the dimensionless parameters, if $G\to0$, $N\to\infty$, $D_0\to0$, or $\gamma\to-1$. If there are no Faradaic reactions, the leading order of the XDL admittance [Eq. (66)] vanishes and we need to go to order ω. We obtain in this case

$$f_1 = \frac{1}{1+\lambda_s} + O(\omega^{1/2}), \quad f_2 = \frac{\gamma^2\sqrt{i\omega}}{1+\lambda_s} + O(\omega),$$

$$Y = \frac{i\omega(1-\gamma^2)}{1+\lambda_s} + O(\omega^{3/2}), \tag{68}$$

$$Z(\text{dim})|_{R_{ct}\to\infty} = \frac{\lambda_D}{\sigma}\bar{Z} = \frac{1}{i\omega}\left(\frac{\lambda_D}{\varepsilon} + \frac{\lambda_s}{\varepsilon_s}\right). \tag{69}$$

The equivalent circuit in this limit is a capacitor with (dimensional) specific capacitance given by $(\lambda_s/\varepsilon_s+\lambda_D/\varepsilon)^{-1}$, i.e., the association in series of the compact and diffuse layers, with negligible contribution of the diffusion layer.

Another distinguished limit from the general, low-frequency, solution corresponds to the facile kinetic regime, characterized by a negligible charge transfer resistance ($G \to \infty$). In this limit the only factors blocking the reaction are the Warburg impedances and we have

$$Z = \frac{W}{(1+\gamma)\sqrt{i\omega}}, \quad f_1 = \frac{1}{1+\lambda_s}\left(1+\frac{\gamma}{W}\right), \quad f_2 = -\frac{\gamma}{W}. \tag{70}$$

In this limit, the voltage drop in the diffusion layer is of the same order as in the diffuse part and of opposite sign.

A uniform solution, valid for both high and low reaction resistances and Warburg impedance, can be obtained from the complete solution assuming temporarily that $G \sim \omega^{1/2}/W \sim \omega$,

$$Y = \frac{1+\gamma}{\frac{1}{G}+\frac{W}{\sqrt{i\omega}}} + \frac{1-\gamma^2}{1+\lambda_s} i\omega, \tag{71}$$

$$f_1 = \frac{1-f_2}{1+\lambda_s}, \quad f_2 = -\frac{\gamma}{\sqrt{i\omega}\left(\frac{1}{G}+\frac{W}{\sqrt{i\omega}}\right)} + \frac{\gamma^2\sqrt{i\omega}}{1+\lambda_s}. \tag{72}$$

This admittance corresponds to a Randles circuit [19] formed by two elements in parallel: a capacitor and a series association of a resistor and a Warburg impedance.

V. ELECTRO-OSMOTIC SLIP VELOCITY

A. General applied ac signal

Once we have calculated the solution for the electric potential inside the XDL, as a function of the total voltage drop, we can integrate Stokes equations to obtain an expression for the electro-osmotic slip velocity. The boundary condition for the velocity at the OHP is that of no slip,

$$u = 0, \quad w = 0. \tag{73}$$

The slip velocity expression is obtained assuming that the normal component of the velocity is very small, $w=0$, across the whole XDL (since we have a thin layer) and that normal derivative of the tangential velocity vanishes for large y, $\partial u/\partial y \to 0$ (as the normal derivatives are much smaller outside the XDL than inside it). After integration, the slip electro-osmotic velocity is the limit of u for large y.

In the thin-layer approximation, the time average of the normal component of the Stokes equation [Eq. (20)] can be written as

$$\frac{\partial\langle p\rangle}{\partial y} = -\rho\frac{\partial\phi^*}{\partial y} - \rho^*\frac{\partial\phi}{\partial y} = \frac{\partial^2\phi}{\partial y^2}\frac{\partial\phi^*}{\partial y} + \frac{\partial^2\phi^*}{\partial y^2}\frac{\partial\phi}{\partial y} = \frac{\partial}{\partial y}\left(\left|\frac{\partial\phi}{\partial y}\right|^2\right), \tag{74}$$

which can be integrated once to give an expression for the time-averaged pressure of electrical origin,

$$\langle p\rangle = p_o + \int_\infty^y \frac{\partial}{\partial y}\left(\left|\frac{\partial\phi}{\partial y}\right|^2\right)dy = p_o + \left|\frac{\partial\phi}{\partial y}\right|^2\Bigg|_\infty^y = p_o + \left|\frac{\partial\phi}{\partial y}\right|^2 - |Y\Delta\Phi|^2, \tag{75}$$

where we have used Eq. (39) for the derivative at the outer limit of the XDL. The expression for the pressure can be inserted in the time average of the tangential Stokes equation [Eq. (19)] to give the second derivative of the tangential liquid velocity inside the XDL,

$$\frac{\partial^2\langle u\rangle}{\partial y^2} = \frac{\partial\langle p\rangle}{\partial x} + \rho^*\frac{\partial\phi}{\partial x} + \rho\frac{\partial\phi^*}{\partial x}. \tag{76}$$

Both the average pressure and the electric volume force are combinations of exponentials that can be integrated to give an expression for the slip velocity as a function of the voltage drop,

$$U = \int_0^\infty\left(\int_\infty^y \frac{\partial^2\langle u\rangle}{\partial y^2}dy\right)dy = A\Delta\Phi\frac{\partial}{\partial x}(\Delta\Phi^*) + B\Delta\Phi\frac{\partial\Phi^*}{\partial x} + \text{c.c.}, \tag{77}$$

with A and B as certain functions of the parameters

$$A = \frac{f_1 f_1^* s_1(s_1-s_1^*)}{(s_1+s_1^*)^2} + \frac{f_1 f_2^* s_1(s_1-s_2^*)}{(s_1+s_2^*)^2} + \frac{f_2 f_1^* s_2(s_2-s_1^*)}{(s_2+s_1^*)^2} + \frac{f_2 f_2^* s_2(s_2-s_2^*)}{(s_2+s_2^*)^2} - \left(\frac{Yf_2^*}{s_2^*}+\frac{Yf_1^*}{s_1^*}\right) - 3\left(\frac{Y^*f_1}{s_1}+\frac{Y^*f_2}{s_2}\right), \tag{78}$$

$$B = f_1 + f_2. \tag{79}$$

The term proportional to A in Eq. (77) connects the voltage drop across the XDL with its tangential derivative. The term proportional to B in Eq. (77) can be interpreted as an extension of the classical Helmholtz-Smoluchowski formula, as is proportional to the tangential field just outside the XDL multiplied by the voltage drop between the OHP and the bulk,

$$U_{HS} \simeq (f_1+f_2)\Delta\Phi\frac{\partial\Phi^*}{\partial x} + \text{c.c.} = -(\Delta\phi_{\text{diffuse}} + \Delta\phi_{\text{diffusion}})E_x^* + \text{c.c.} \tag{80}$$

It must be noted, however, that this extension includes the contribution of the diffusion layer. The order of magnitude of

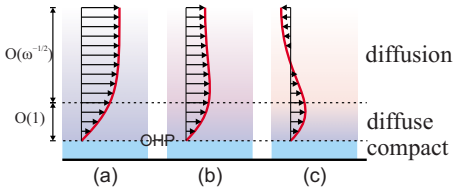

FIG. 4. (Color online) Contributions to the electro-osmotic velocity, (a) $f_2 \ll f_1$ and $\mathrm{sgn}(f_2)=\mathrm{sgn}(f_1)$, (b) $f_2 \ll f_1$ and $\mathrm{sgn}(f_2)=-\mathrm{sgn}(f_1)$, and (c) $f_2 \sim f_1$ and $\mathrm{sgn}(f_2)=-\mathrm{sgn}(f_1)$, where f_1 and f_2 are proportional to the voltage drop across the diffuse and diffusion layers, respectively. In the first and second cases, the effect of the diffusion layer is small and cannot reverse the flow. In the third case, the diffusion layer stresses can overcome the diffuse layer ones and produce flow reversal.

the voltage drop across the diffusion layer compared to the diffuse layer is critical. When f_2/f_1 is of order unity, the diffusion layer can reinforce, reduce, or even reverse the electro-osmotic velocity produced by the diffuse layer (Fig. 4).

The coefficients A and B that appear in the electro-osmotic velocity [Eq. (77)] have the values, in the low-frequency domain,

$$A = f_2^*\left(f_1 - \frac{Y}{\sqrt{-i\omega}}\right) - f_2\left(\frac{1-i}{2}f_2^* + \frac{3Y^*}{\sqrt{i\omega}}\right), \quad B = f_1 + f_2. \tag{81}$$

We can see that if the voltage drop in the diffusion layer is negligible ($f_2 \to 0$), the coefficient A becomes negligible too and the electro-osmotic velocity reduces to the usual Helmholtz-Smoluchowski formula. This happens in particular in two important cases: for a totally symmetric electrolyte ($\gamma=0$) and for perfectly polarizable electrodes. In the first case, $\gamma=0$ implies that $f_2=0$. In the second case, the Faradaic currents are blocked [Eq. (68)] and, in this limit, the coefficients become

$$A = \frac{\gamma^2\sqrt{i\omega}}{1+\lambda_s} + O(\omega), \quad B = \frac{1}{1+\lambda_s} + O(\omega^{1/2}). \tag{82}$$

A is of order $\omega^{1/2}$, negligible in front of B, and the electro-osmotic velocity reduces again to the Helmholtz-Smoluchowski formula

$$U = \frac{1}{1+\lambda_s}\left(\Delta\Phi^*\frac{\partial\Phi}{\partial x} + \text{c.c.}\right). \tag{83}$$

Another distinguished limit is the facile kinetic regime. In this case, the coefficients become

$$A = \frac{-2\gamma W - \gamma^2(3+\lambda_s) + (4+3\gamma)(1+\lambda_s)\gamma i}{2(1+\lambda_s)W^2},$$

$$B = \frac{1}{1+\lambda_s}\left(1 - \frac{\lambda_s\gamma}{W}\right). \tag{84}$$

We can see that the coefficient B, which produces a term in the form of generalized Helmholtz-Smoluchowski formula (80), can change sign for large compact layer thicknesses λ_s or asymmetries. This change in sign is at the origin of the change in sign of the electro-osmotic slip velocity. However, the coefficient A has a more complex structure and the net result must be analyzed on a case by case basis since the total voltage drop $\Delta\Phi$ and the voltage outside the XDL, Φ, vary in different forms for each electrode distribution and applied wave form. In Sec. V B we will solve the particular case of a traveling-wave voltage.

B. Case of a traveling-wave signal

Once we have a complete expression for the electro-osmotic slip velocity as a function of the electric potential in the bulk, we can proceed to apply it to a particular problem. In what follows we consider the case of a single mode traveling-wave signal. For this case, we take as typical tangential length L the wavelength divided by 2π, so that the dimensionless complex amplitude of the applied signal is

$$V_s = \frac{V_0}{2}e^{-ix}. \tag{85}$$

In this problem, the bulk is electroneutral and the electric potential outside the XDL verifies Laplace equation

$$\frac{\partial^2\Phi}{\partial x^2} + \frac{\partial^2\Phi}{\partial y_o^2} = 0, \tag{86}$$

with $y_o=\delta y$ as the bulk normal length. Solving Eq. (86) with boundary condition (51) and the condition that the potential vanishes far from the electrodes, we obtain the potential in the bulk, just outside the XDL and total voltage drop,

$$\Phi(y) = \frac{YV_0e^{(-ix-y_o)}}{2(\delta+Y)}, \quad \Phi = \frac{YV_0e^{-ix}}{2(\delta+Y)}, \quad \Delta\Phi = \frac{\delta V_0e^{-ix}}{2(\delta+Y)}. \tag{87}$$

The resulting electro-osmotic velocity is independent of position and equal to

$$U = \frac{\delta V_0^2}{2|\delta+Y|^2}\mathrm{Im}(\delta A + BY). \tag{88}$$

For any value of frequency, U is obtained through the expressions of A and B [Eqs. (78) and (79)] as functions of f_1, f_2, and Y, which are given by the solution in the thin-layer approximation (see Appendix B). The maximum electro-osmotic velocity will occur for frequencies where $Y=O(\delta)$ (if it is of order 1 and U is order δ). In the ideally polarizable limit, where $Y=i\omega C$, this maximum happens for $\omega \sim \delta$. In the facile kinetic regime, where Y is dominated by the Warburg impedance $Y \sim (i\omega)^{1/2}$ and the maximum response lies in the $\omega \sim \delta^2$ range, i.e., for lower frequencies. For intermediate cases, as we will see, we can have a peak at an intermediate frequency or two coexisting maxima.

VI. RESULTS

A. Ideally polarizable electrodes

The first parameter we explore is asymmetry in the absence of Faradaic reactions ($G=0$).

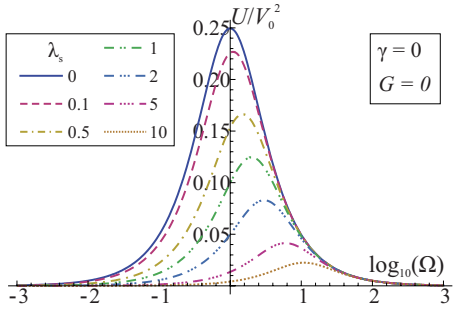

FIG. 5. (Color online) Slip velocity for equal diffusivities and ideally polarizable electrodes for different compact layer thicknesses λ_s. Increasing λ_s results in smaller slip velocity and a displacement of the maximum to higher frequencies.

Figure 5 shows the velocity as a function of frequency Ω for different compact layer thicknesses λ_s. The combined effect of compact layer thickness and asymmetry is shown in Fig. 6. We employ the nondimensional frequency Ω, which is given by the product of the angular frequency times the relaxation time of the *RC* circuit formed by the double layer and the bulk, $\Omega=[\omega(\mathrm{dim})\varepsilon/\sigma](L/\lambda_D)=\omega(1-\gamma^2)/\delta$.

We can see that the effect of asymmetry is too small to be considered even for high values of γ.

From this result we established previously that the diffusion layer has negligible contribution to both the XDL impedance and the total voltage drop, i.e.,

$$U=\frac{V_0^2\,\mathrm{Im}(Y/\delta)}{2(1+\lambda_s)|1+Y/\delta|^2}. \tag{89}$$

For this case, the XDL admittance, which does include contributions from the diffusion layer in addition to the double layer, reduces to a pure capacitor, $Y=i\omega(1-\gamma^2)=i\Omega\delta$, and the slip velocity reduces to the well-known case $U=\Lambda V_0^2\Omega/[2(1+\Omega^2)]$, with $\Lambda=f_1=1/(1+\lambda_s)$ [9].

B. Faradaic currents with and without asymmetry

If we include Faradaic currents in the model, the number of parameters is increased in three: the reaction conductance G, the relative concentration N, and the neutral diffusivity D_0, although, as we stated previously, the combination

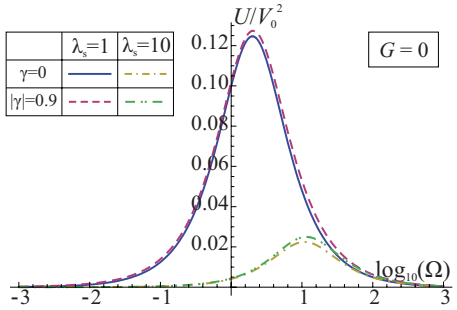

FIG. 6. (Color online) Slip velocity for ideally polarizable electrodes, with different compact layer thicknesses and with and without asymmetry. The effect of asymmetry is almost negligible in this case of zero Faradaic currents.

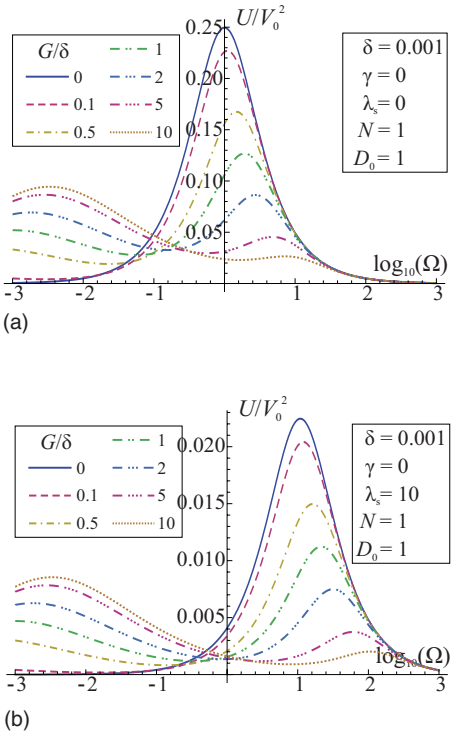

FIG. 7. (Color online) Slip velocity in the presence of Faradaic currents, with (a) a small compact layer and (b) a large one, for equal ion mobilities. When the resistance to reaction decreases there appears a secondary maximum at low frequencies, associated to the Warburg impedance and characterized, in dimensionless form, condition $\omega^{1/2}\sim\delta$. For a thick compact layer, the primary maximum is displaced and lowered compared with the case $\lambda_s=0$, as in Fig. 5, due to the increase in compact layer thickness (notice the different vertical scales). The secondary maximum also reduces its amplitude, but the position of the maximum is not greatly affected by the change in λ_s.

$N/D_0^{1/2}$ works as a single parameter. In the case of a symmetric solution ($\gamma=0$) we see that the presence of Faradaic currents produces a secondary bell at lower frequencies (Fig. 7). The presence of a thick compact layer reduces the voltage drop across the diffuse layer, lowering the electro-osmotic velocity. In addition, the primary maximum is displaced to higher frequencies, but the frequency of the secondary maximum (associated to the Warburg impedance) is not affected. Notice that we use G/δ as parameter that controls the reactions rather than G. The parameter G/δ is the reaction conductance made nondimensional using the bulk scale L rather than the Debye length, $G/\delta=LK_+/2D_+$. The reciprocal of G/δ is the same parameter that was used in [19], except for the factor $(1+\gamma)$, to describe the nondimensional reaction resistance R_s and, in this way, we can see that Fig. 7 is totally coincident with previous results for $\gamma=0$.

Figure 8 shows that the effect of reducing the equilibrium concentration of neutral species (raising the value of N) or its diffusivity is twofold: displaces the position of the secondary maximum to higher frequencies and blocks the reaction until the two maxima coalesce and the system is indistinguishable from an ideally polarizable electrode.

Now, let us consider the combined effect of Faradaic currents and asymmetry. As we have stated previously, the pres-

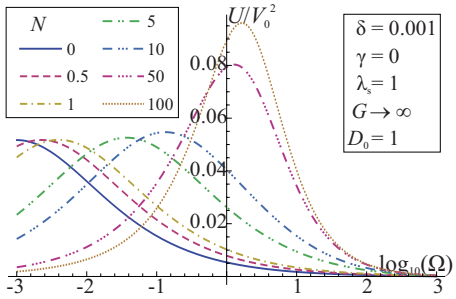

FIG. 8. (Color online) Effect of concentration of neutral species on slip velocity for equal ion mobilities with vanishing reaction resistance. For small N (bath of neutral species), the behavior is dominated by diffusion of the charged species. For large N (scarce neutral species) the reaction is blocked and the system behaves as an ideally polarizable one.

ence of asymmetry implies a charge density and a voltage drop across the diffusion layer. It should be noted that we must be careful in extending our analysis to ultralow frequencies because then the diffusion layer thickness gets to be of the order of the macroscopic bulk scale and the thin-layer approximation ceases to be valid. Nevertheless, for the case of a single mode traveling wave, it is possible to find a complete linear solution, including the potential in the bulk (see Appendix C). Figure 9 shows the calculated slip velocity using the complete and thin-layer models. We can see that, as long as $\Omega > 10^{-1}$ (that corresponds to a dimensional frequency of around 10 Hz), both curves coincide. The thin-

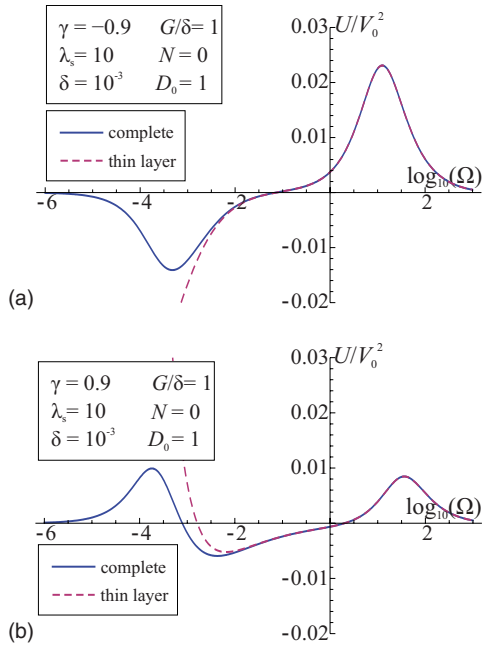

FIG. 9. (Color online) Comparison of the complete linear analysis (solid line) and the thin-layer approximation (dashed line) for (a) negative and (b) positive asymmetries in the presence of Faradaic currents. The approximate solution has a catastrophic behavior for very low frequencies, but the complete solution shows that this is just a consequence of the approximations made and that the divergence does not happen in the regions of physical interest (for $\Omega \geq 10^{-2}$).

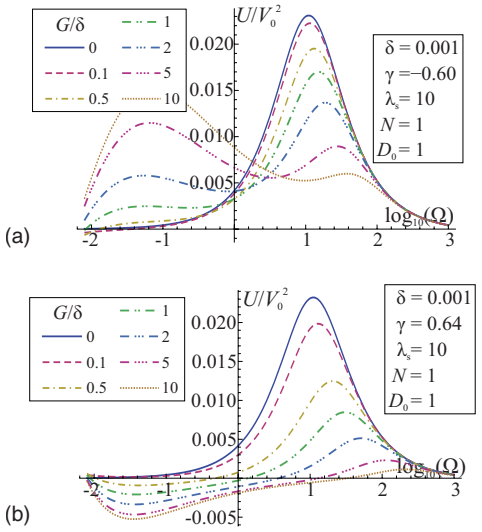

FIG. 10. (Color online) Dependence of the electro-osmotic velocity with the reaction conductance for a negative asymmetry [(a) case of NaOH] and a positive one [(b) case of HCl]. When the more mobile species is the nonreacting one, there is not predicted reversal except for extremely low frequencies (in dimensional form, around 1 Hz or less). If the more mobile species is the reacting one, the model predicts reverse flow when the reaction resistance is low enough.

layer approximation produces a catastrophic region at ultralow frequencies, which is not present in the complete solution. In fact, the complete analysis shows that the slip velocity goes to zero for very low frequencies, as should be expected.

Despite the reduced frequency range of validity, the thin-layer approximation has the advantage of being easily extensible to different problems through the Robin-type boundary condition (51) stated previously. Here, contrary to the conclusions in [27], the thin-layer approximation and the full linear solution coincide nicely for $\delta \sim 0.01-0.001$.

Figure 9 shows a prominent feature of electro-osmotic slip velocity under the combined effects of Faradic currents and different mobilities: *it predicts reverse flow* since there are ranges of frequencies where the curve is below the X axis, and although these ranges are in the very low-frequency region, they fall in the domain of validity of the thin-layer approximation. Notice that the magnitude of the reverse flow velocity is very small.

We now explore the effect of three different parameters (reaction resistance, asymmetry, and compact layer thickness) on the flow, with particular attention on the flow reversal.

Figure 10(a) shows the effect of the reaction conductance for an electrolyte with a negative asymmetry $\gamma = -0.60$ (the case of Na^+OH^-), while Fig. 10(b) shows the effect for a positive asymmetry of $\gamma = +0.64$ (the case of H^+Cl^-). We can see that the reverse flow happens for high values of the conductance G/δ (the facile kinetic regime). Only if the more mobile ion is the reacting one, $\gamma > 0$, the region of negative velocities includes frequencies Ω of order 1. This last point is illustrated in Fig. 11, where we vary the asymmetry parameter γ for a given reaction resistance. We can see that the

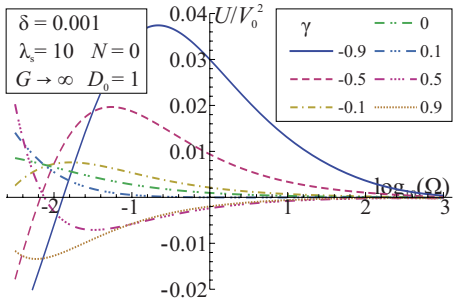

FIG. 11. (Color online) Dependence on the asymmetry for a solution in the facile kinetic regime ($G \to \infty$). In this limit, the model predicts reverse flow for both limits of the asymmetry, but only in the case in which the reactive ion is the more mobile one ($\gamma \sim +1$), the reverse flow lies in the observable range.

system is very sensitive to changes in the mobility differences and that the reverse flow grows with the asymmetry. For $\gamma < 0$, there is a region of reverse flow but it happens at very low frequencies $\Omega < 0.01$, which may or may not be observable because the oscillating terms are very important and can mask the time-averaged force. For $\gamma > 0$, the region of reverse flow includes frequencies that are typical of ACEO ($\Omega \sim 1$) and, therefore, can be observable.

If we consider the effect of the compact layer thickness (Fig. 12) we see that for thin compact layers there is no reverse flow and that the effect requires a certain thickness.

Combining these three factors, we find that we need a low reaction resistance, a positive asymmetry (being the reacting ion the more mobile), and a thick compact layer. This result can be understood from the analytical expressions in the facile kinetic regime ($R_s \to 0$ or $G \to \infty$).

C. Facile kinetic regime

Next, we assume that $G \to \infty$ (i.e., that the reaction resistance vanishes) so that the only factor blocking the reaction is the diffusion of the reactive species. We obtained previously the XDL impedance and the coefficients A and B for the general electro-osmotic velocity [Eq. (84)]. Inserting

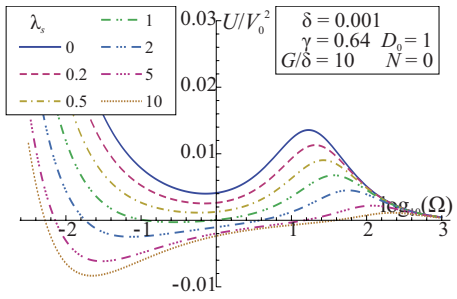

FIG. 12. (Color online) Dependence on the compact layer thickness for a solution with positive asymmetry in the facile kinetic regime. If the compact layer is very thin there is no reverse flow, but if it is of same order or larger than the diffuse layer, there could be flow reversal since the voltage drop in the diffuse (Debye) layer is greatly reduced and can be overcome by the opposite voltage drop across the diffusion layer.

these in Eq. (88) we obtain the electro-osmotic slip velocity in the facile kinetic regime,

$$U = \frac{\delta V_0^2[(4+3\gamma)\gamma\delta(1+\lambda_s) + (W-\lambda_s\gamma)(1+\gamma)\sqrt{2\omega}]}{2(1+\lambda_s)|\delta W + (1+\gamma)\sqrt{i\omega}|^2}. \tag{90}$$

The minus sign in the numerator can change the direction of the velocity if the asymmetry and the compact layer thickness are large enough.

An easier explanation can be argued considering the case of a bath of neutral species ($N=0$), where the only Warburg impedance comes from the charged species, so that $W=1-\gamma$. In this case, the low-frequency solution [Eq. (70)] implies that the voltage drop across the diffusion layer is of opposite sign to that of the diffuse layer. In particular

$$f_1 \simeq \frac{1}{(1-\gamma)(1+\lambda_s)}, \quad f_s \simeq \frac{\lambda_s}{(1-\gamma)(1+\lambda_s)}, \quad f_2 \simeq -\frac{\gamma}{1-\gamma}. \tag{91}$$

The coefficient B that gives the generalized Helmholtz-Smoluchowski contribution to the slip velocity reduces to

$$B = \frac{1}{1+\lambda_s}\left(1 - \frac{\lambda_s\gamma}{1-\gamma}\right) \tag{92}$$

and changes sign if $\gamma > 1/(1+\lambda_s)$. Given the typical values of γ in nature, the ratio $1/(1+\lambda_s)$ should be small in order to have this change of sign or, equivalently, λ_s should be much greater than 1.

D. Relation to experimental values

In order to compare with experimental results, we should assign specific numerical values to the different parameters of the linear theory. García-Sánchez *et al.* [21] showed changes in *p*H for typical signals of reverse flow and it was inferred that chemical reactions of the H^+ ion were taking place at the electrodes. It was also assumed that the majority of positive ions near the electrodes were H^+ ions. Therefore, we are going to consider in our linear model that the binary electrolyte is HCl with a concentration of 0.1 mM. The diffusivity asymmetry for the pair H^+Cl^- has the value $\gamma = +0.642$ (from [28]), showing that the hydrogen ion is much more mobile than the chloride ion. For a 0.1 mM solution at 300 K, the Debye length is $\lambda_D = (\varepsilon k_B T/2e^2 c^{eq})^{1/2} \approx 30$ nm while the conductivity of the solution is $\sigma = \varepsilon D/[\lambda_D^2(1-\gamma^2)] \approx 4.4$ mS/m. For the four-phase electrode array used in experiments, the wavelength was 160 μm, which leads to $L = 160/(2\pi)$ μm ≈ 25 μm as the typical length (therefore, $\delta = 1.2 \times 10^{-3}$). The characteristic angular frequency used to scale the applied signal frequency is $\omega_0 = \lambda_D \sigma/\varepsilon L \approx 7400$ s^{-1} ($f_0 = \omega_0/2\pi \approx 1200$ Hz). For this frequency, the thickness of the diffusion layer is in the range of $(D/\omega_0)^{1/2} \approx 0.68$ μm. The value of the parameter λ_s is more difficult to estimate since requires knowledge of the internal structure of the double layer. We are going to choose a typical value of $\lambda_s = 4$, which was used in Refs. [12,29,30] in order to fit the predictions of the linear model to the experimental velocities.

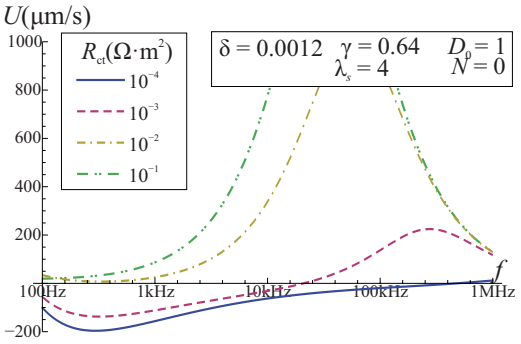

FIG. 13. (Color online) Dimensional results for the case discussed in Sec. VI D. The parameters correspond to a 0.1 mM solution of HCl in water over an electrode array of wavelength 160 μm.

We set the value of the voltage amplitude to 1 V, which gives a nondimensional voltage $V_0 \approx 40$. Since we are considering an aqueous solution and the charged reacting species is hydrogen H^+, the neutral species is just water. In this case, we can make $N \approx 0$, i.e., the ratio of ion concentration (H^+) to neutral species concentration (water) is negligible. With these parameters, we obtain the graph shown in Fig. 13. For a charge transfer resistance $R_{ct}=10^{-4}$ Ω m^2 the velocity around 1 kHz is in the direction of the reverse flow and of the order of 150 μm/s. This value of the charge transfer resistance is much smaller than the typical bulk specific resistance ($L/\sigma=57\times10^{-4}$ Ω m^2) and, therefore, in the limit of facile kinetics. The computed reverse flow appears in the range of typical frequencies of the experimental observations, showing a decrement with increasing frequency in qualitative agreement with experiments. The velocity amplitudes computed with this set of parameters are high enough to be observable and, therefore, the mechanism analyzed here (i.e., electrical forces in the diffusion layer due to different ion mobilities) should be considered as a candidate to explain the observed reverse flows in TWEO experiments.

VII. CONCLUSIONS

The present study shows that the linear analysis can predict reverse flow in traveling-wave electro-osmosis if three conditions occur simultaneously: the Faradaic reactions are facile, the mobilities of the species are different (with the reacting ion as the most mobile one), and the compact layer is not very thin compared to the diffuse layer.

The difference in mobilities is necessary for charge and voltage drop to exist in the diffusion layer above the double layer. This voltage drop can be of opposite sign to that across the diffuse layer and then can reverse the flow if it is large enough.

The facile kinetic regime relates the behavior of the mean ion concentration to the charge density, making the voltage drop across the diffusion layer of the same order as the diffuse one. In the opposite case, of an ideally polarizable electrode, $\Delta\phi_{\text{diffusion}}$, albeit present, is much smaller than $\Delta\phi_{\text{diffuse}}$ and cannot produce flow reversal.

Finally, the presence of a thick compact layer reduces the voltage drop across the diffuse layer since most of the voltage drop in the double layer happens at the compact layer. The combination of the three factors together allows for the occurrence of flow reversal. The characteristic frequencies at which the maximum reversal occurs are low and associated to the Warburg impedance.

We acknowledge that this linear model cannot be the whole explanation of the observed flow reversal in TWEO, which is clearly a nonlinear phenomenon, happening only when a certain voltage threshold is reached. However, the fact that it predicts flow reversal for frequencies typical of experiments is important. It also requires that the more mobile ion is the reacting one, which is supported by the experimental observation of production of H^+ at the electrodes for typical voltages of reversal [21]. All these facts suggest that this model can be part of the explanation. Our solutions for reverse flow require that the reaction resistance is small. This is a regime that can be reached by increasing voltage, given that the exponential growth of Faradaic currents with voltage means that the equivalent reaction resistance gets to be very small. The experimental observations of flow reversal in TWEO for voltages greater than a certain threshold [20,21] suggest the relation with the onset of Faradaic reactions.

The flow reversal described here could be related to the experimental observations by Gregersen *et al.* [14]. In particular, the velocity dependence with frequency at constant voltage for 4 mS/m KCl [inset in their Fig. 4(a)] is reminiscent of the reverse flow behavior shown here in our Figs. 10(b) and 12. The analysis developed on our work for TW potentials should then be extended to the case of ac potentials applied to asymmetric pairs of electrodes.

An important feature of our solutions is that it is required λ_s to be large in order to obtain reverse flow. Typical values of capacity of diffuse and compact layers do not produce $\lambda_s > 1$ except for high electrolyte conductivity. However, experiments in ac electro-osmosis [3,9,12,29,30] show that the linear theory overestimates the slip velocity or, otherwise, that the voltage across the diffuse layer is less than expected. The presence of steric effects [15–17,30] at voltages much greater than $k_BT/e=0.025$ V could be important in this case. The ion crowding of the double layer at high voltages may be modeled as a condensed layer of variable thickness. This condensed layer would act as the compact layer in our problem: not contributing to the electro-osmotic velocity and thus allowing the stresses in the diffusion layer to overcome the stresses in the diffuse layer and reverse the flow.

We have performed the analysis in the thin-layer approximation. Although this approximation is questionable for very low frequencies, it may provide an easier generalization to different problems as the case of two coplanar electrodes or arrays of electrodes subjected to four-phase signals, as the ones used in the experiments, using boundary condition (51) for the outer problem and inserting the result in Eq. (77) to obtain the slip velocity.

ACKNOWLEDGMENTS

This work was supported by the Spanish Government Agency DGCyT and Junta de Andalucía under Contracts No. FIS2006-03645 and No. FQM-241, respectively.

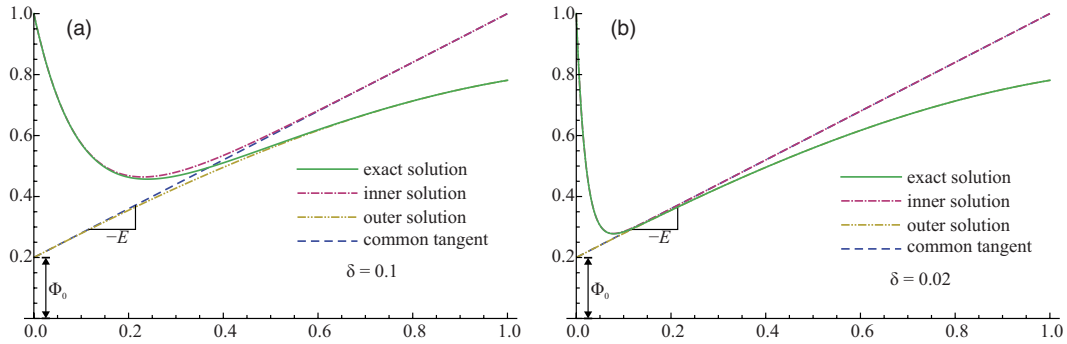

FIG. 14. (Color online) Illustration of the matching condition for two values of a small parameter using as example the function $y=0.8\exp(-x/\delta)+0.2\sin(x)+0.5\cos(x)$. Notice that Φ_0 is the point where the straight line crosses the x axis and can be different from the value of the potential on the intermediate region.

APPENDIX A: MATCHING CONDITION

The matching conditions (29) and (30) can be derived in a general way using the matched asymptotic expansion method (see, for instance, [31]). In this case, however, we can give a simple geometrical interpretation (Fig. 14).

We have to match the *inner solution*, ϕ, valid inside the XDL, which varies in a scale of order l, with the *outer solution*, Φ, which varies typically with a macroscopic length L, much greater than l. In a first-order perturbative analysis, we solve for each region with an error of the order of $\delta=l/L$. The matching conditions are given by the requirement that in an *intermediate scale* (much larger than l and much smaller than L) both solutions coincide up to this order.

The one-dimensional equations inside the double layer reduce to a vanishing second derivative for the electric potential when we move from the XDL to the electroneutral bulk. That means that the inner solution is a combination of exponentially decreasing terms plus a linear behavior. We see that just outside the XDL the inner solution is a straight line $\phi \sim \Phi_0 - Ey$ $(y \gg l)$.

The matching condition requires this straight line to coincide with the outer solution on the same intermediate scale; i.e., the straight line must be asymptotically tangent to the outer solution evaluated at positions with $y \ll L$ (i.e., effectively at $y_o \to 0$, being $y_o = y/L$). The slope and the intersection with the axis must be the same for both solutions,

$$\lim_{y\to\infty}\frac{d\phi}{dy} = -E = \lim_{y\to 0}\frac{d\Phi}{dy}, \tag{A1}$$

$$\lim_{y\to\infty}\left(\phi - y\frac{d\phi}{dy}\right) = \Phi_0 = \lim_{y\to 0}\left(\Phi - y\frac{d\Phi}{dy}\right) = \lim_{y\to 0}\Phi. \tag{A2}$$

APPENDIX B: VALUES OF THE COEFFICIENTS

The values for the fraction of voltage drops in Eqs. (52)–(60) subjected to condition (43) can be calculated from the admittance,

$$Y = (1+\gamma)\omega^2 s_1 s_2\left(\frac{a+Gb}{c+G(d+eN_0 s_0)}\right), \tag{B1}$$

$$a = \omega(1-\gamma)(\Gamma^2-\gamma^2\omega^2), \tag{B2}$$

$$b = -i[(\lambda_s+Ns_0)(\Gamma^2-\gamma^2\omega^2)+(\Gamma-i\gamma\omega)^2 s_1+(\Gamma+i\gamma\omega)^2 s_2], \tag{B3}$$

$$c = (1-\gamma)\omega[\omega^2\gamma^2 s_1^3-\Gamma s_2^3-\lambda_s(\Gamma^2-\gamma^2\omega^2)s_1^3 s_2^3], \tag{B4}$$

$$d = -i(1-\gamma)\omega^2[(\Gamma^2-\gamma^2\omega^2)+\lambda_s(\Gamma+i\gamma\omega)^2 s_1^3 + \lambda_s(\Gamma-i\gamma\omega)^2 s_2^3], \tag{B5}$$

$$e = -i[s_1^3\gamma^2\omega^2 - s_2^3\Gamma^2 - \lambda_s s_1^3 s_2^3(\Gamma^2-\gamma^2\omega^2)], \tag{B6}$$

through the expressions

$$f_1 = f_{10}+f_{11}Y, \quad f_2 = f_{20}+f_{21}Y, \tag{B7}$$

$$f_{10} = \frac{1}{P_1 M}, \quad f_{20} = \frac{1}{P_2 M}, \quad M = \frac{1+\lambda_s s_1}{P_1}+\frac{1+\lambda_s s_2}{P_2}, \tag{B8}$$

$$P_1 = i\omega\gamma(\Gamma+i\omega\gamma)s_1, \quad P_2 = \Gamma(\Gamma-i\omega\gamma)s_2, \tag{B9}$$

$$f_{11} = \frac{1}{Q_1 T}, \quad f_{21} = \frac{1}{Q_2 T}, \quad T = -\frac{1+\lambda_s s_1}{\lambda_s Q_1}-\frac{1+\lambda_s s_2}{\lambda_s Q_2}, \tag{B10}$$

$$Q_1 = \lambda_s P_1 - (1+\lambda_s s_1)\frac{\Gamma\gamma}{1+\gamma}, \quad Q_2 = \lambda_s P_2 + (1+\lambda_s s_2)\frac{\Gamma\gamma}{1+\gamma}, \tag{B11}$$

where

$$\Gamma = \frac{1+\sqrt{1-4\gamma^2\omega^2}}{2}, \quad s_1 = \sqrt{\Gamma+i\omega}, \quad s_2 = \sqrt{1+i\omega-\Gamma}. \tag{B12}$$

The rest of the quantities are obtained from the voltage drops as

$$\rho_1 = -(\Gamma+i\omega)f_1, \quad n_1 = -\frac{i\omega\gamma}{\Gamma}\rho_1, \quad n_2 = -\frac{\Gamma-i\gamma^2\omega}{\gamma}f_2, \quad \rho_2 = \frac{i\omega\gamma}{\Gamma}n_2, \tag{B13}$$

$$f_s = 1 - f_1 - f_2, \quad a_0 = -\frac{N(s_1 n_1 + s_2 n_2)}{D_0(1-\gamma)s_0}. \tag{B14}$$

APPENDIX C: COMPLETE SINGLE MODE TRAVELING WAVE SOLUTION

In the particular case of a single mode traveling-wave electro-osmosis the problem can be solved completely, including the potential in the bulk. The electric potential can be written for this case as

$$\phi = \left(f_1 e^{-s_1 y} + f_2 e^{-s_2 y} + \frac{Y}{\delta} e^{-\delta y} \right) \Delta\Phi(x), \tag{C1}$$

where

$$\Delta\Phi(x) = \frac{\delta e^{-ix}}{2(\delta + Y)}, \quad \Phi(x) = \frac{Y}{\delta}\Delta\Phi = \frac{Y e^{-ix}}{2(\delta + Y)} \tag{C2}$$

(the notation has been chosen to maximize the coincidence with the thin-layer approximation). The charge density and excess in the mean concentration are formally the same as in Eqs. (40) and (41). The new exponents satisfy

$$s_i^2 = s_{Ti}^2 + \delta^2, \tag{C3}$$

with s_T as the corresponding exponents in the thin-layer approximation, given in Eqs. (46)–(48).

The system of equations for the coefficients is exactly the same as in Eqs. (52)–(60), hence the analytic solution is the same as in Appendix B (using the new exponents, although Γ is unchanged).

The expression for the slip velocity is the same as in Eq. (88) where now

$$\mathrm{Im}(\delta\alpha + \beta Y) = \frac{\delta}{2i}\left(\frac{f_1 f_1^*(s_1^{*2} - s_1^2)}{(s_1 + s_1^*)^2} + \frac{f_2 f_1^*(s_1^{*2} - s_2^2)}{(s_2 + s_1^*)^2} + \frac{f_1 f_2^*(s_2^{*2} - s_1^2)}{(s_1 + s_2^*)^2} + \frac{f_2 f_2^*(s_2^{*2} - s_2^2)}{(s_2 + s_2^*)^2} + \frac{Y f_1^*(s_1^{*2} - \delta^2)}{\delta(s_1^* + \delta)^2} + \frac{Y f_2^*(s_2^{*2} - \delta^2)}{\delta(s_2^* + \delta)^2} - \frac{Y^* f_1(s_1^2 - \delta^2)}{\delta(s_1 + \delta)^2} - \frac{Y^* f_2(s_2^2 - \delta^2)}{\delta(s_2 + \delta)^2} \right), \tag{C4}$$

while the corresponding expression in the thin-layer approximation (with the appropriate exponents) is

$$\mathrm{Im}(\delta\alpha + \beta Y) = \frac{\delta}{2i}\left[\frac{f_1 f_1^*(s_1^{*2} - s_1^2)}{(s_1 + s_1^*)^2} + \frac{f_2 f_1^*(s_1^{*2} - s_2^2)}{(s_2 + s_1^*)^2} + \frac{f_1 f_2^*(s_2^{*2} - s_1^2)}{(s_1 + s_2^*)^2} + \frac{f_2 f_2^*(s_2^{*2} - s_2^2)}{(s_2 + s_2^*)^2} + \frac{Y f_1^*}{\delta}\left(1 - \frac{2\delta}{s_1^*}\right) + \frac{Y f_2^*}{\delta}\left(1 - \frac{2\delta}{s_2^*}\right) - \frac{Y^* f_1}{\delta}\left(1 - \frac{2\delta}{s_1}\right) - \frac{Y^* f_2}{\delta}\left(1 - \frac{2\delta}{s_2}\right) \right]. \tag{C5}$$

The main differences between both expressions is given by the fact that in the complete linear solution s_2 does not goes to zero nor Y to infinity in the limit $\omega \to 0$, preventing the singular behavior for ultralow frequencies.

[1] A. Ramos, H. Morgan, N. G. Green, and A. Castellanos, J. Colloid Interface Sci. **217**, 420 (1999).
[2] A. González, A. Ramos, N. G. Green, A. Castellanos, and H. Morgan, Phys. Rev. E **61**, 4019 (2000).
[3] N. G. Green, A. Ramos, A. González, H. Morgan, and A. Castellanos, Phys. Rev. E **61**, 4011 (2000).
[4] H. Stone, A. Stroock, and A. Ajdari, Annu. Rev. Fluid Mech. **36**, 381 (2004).
[5] T. M. Squires and S. R. Quake, Rev. Mod. Phys. **77**, 977 (2005).
[6] A. B. D. Brown, C. G. Smith, and A. R. Rennie, Phys. Rev. E **63**, 016305 (2000).
[7] V. Studer, A. Pepin, Y. Chen, and A. Ajdari, Analyst **129**, 944 (2004).
[8] B. P. Cahill, L. J. Heyderman, J. Gobrecht, and A. Stemmer, Phys. Rev. E **70**, 036305 (2004).
[9] A. Ramos, H. Morgan, N. G. Green, A. González, and A. Castellanos, J. Appl. Phys. **97**, 084906 (2005).
[10] M. Z. Bazant and T. M. Squires, Phys. Rev. Lett. **92**, 066101 (2004).
[11] T. M. Squires and M. Z. Bazant, J. Fluid Mech. **509**, 217 (2004).
[12] N. G. Green, A. Ramos, A. González, H. Morgan, and A. Castellanos, Phys. Rev. E **66**, 026305 (2002).
[13] P. García-Sánchez, A. Ramos, N. G. Green, and H. Morgan, IEEE Trans. Dielectr. Electr. Insul. **13**, 670 (2006).
[14] M. M. Gregersen, L. H. Olesen, A. Brask, M. F. Hansen, and H. Bruus, Phys. Rev. E **76**, 056305 (2007).
[15] M. S. Kilic, M. Z. Bazant, and A. Ajdari, Phys. Rev. E **75**, 021502 (2007).
[16] M. S. Kilic, M. Z. Bazant, and A. Ajdari, Phys. Rev. E **75**, 021503 (2007).
[17] B. D. Storey, L. R. Edwards, M. S. Kilic, and M. Z. Bazant, Phys. Rev. E **77**, 036317 (2008).
[18] L. H. Olesen, H. Bruus, and A. Ajdari, Phys. Rev. E **73**, 056313 (2006).
[19] A. Ramos, A. González, A. Castellanos, and P. García-Sánchez, J. Colloid Interface Sci. **309**, 323 (2007).

[20] P. García-Sánchez, A. Ramos, N. G. Green, and H. Morgan, Langmuir **24**, 9361 (2008).
[21] P. García-Sánchez, A. Ramos, A. González, N. G. Green, and H. Morgan, Langmuir **25**, 4988 (2009).
[22] J. S. Newman and K. E. Thomas-Alyea, *Electrochemical Systems* (Wiley-IEEE, New York, 2004).
[23] J. O'M. Bockris and A. K. N. Reddy, *Modern Electrochemistry*, 2nd ed. (Springer, New York, 2008).
[24] A. Bonnefont, F. Argoul, and M. Z. Bazant, J. Electroanal. Chem. **500**, 52 (2001).
[25] A. J. Bard and L. R. Faulkner, *Electrochemical Methods: Fundamentals and Applications*, 2nd ed. (Wiley, New York, 2001).
[26] L. Olesen, Ph.D. thesis, Technical University of Denmark, 2006.
[27] M. M. Gregersen, M. B. Andersen, G. Soni, C. Meinhart, and H. Bruus, Phys. Rev. E **79**, 066316 (2009).
[28] David R. Lide (ed.), *CRC Handbook of Chemistry and Physics*, 90th ed. (CRC Press, Boca Raton, 2009) (http://www.hbcpnetbase.com/).
[29] H. Yang, H. Jiang, D. Shang, A. Ramos, and P. García-Sánchez, IEEE Trans. Dielectr. Electr. Insul. **16**, 417 (2009).
[30] M. Z. Bazant, M. S. Kilic, B. D. Storey, and A. Ajdari, Adv. Colloid Interface Sci. **152**, 48 (2009).
[31] J. Kevorkian and J. D. Cole, *Perturbation Methods in Applied Mathematics* (Springer, New York, 1981).